Langmuir Article

pubs.acs.org/Langmuir

The Critical Role of Surfactants in the Growth of Cobalt Nanoparticles

Yuping Bao,*,‡ Wei An,‡ C. Heath Turner,‡ and Kannan M. Krishnan*,†

†*Materials Science & Engineering, University of Washington, Seattle, Washington 98195, and* ‡*Chemical & Biological Engineering, The University of Alabama, Tuscaloosa, Alabama 35487*

Received June 12, 2009. Revised Manuscript Received August 24, 2009

We report a combined experimental and computational study on the critical role of surfactants in the nucleation and growth of Co nanoparticles synthesized by chemical routes. By varying the surfactant species, Co nanoparticles of different morphologies under similar reaction conditions (e.g., temperature and Co−precursor concentration) were produced. Depending on the surfactant species, the growth of Co nanoparticles followed three different growth pathways. For example, with surfactants oleic acid (OA) and trioctylphosphine oxide (TOPO) used in combination, Co nanoparticles followed a diffusional growth pathway, leading to single crystalline nanoparticles. Multiple-grained nanoparticles, through an aggregation process, were formed with the combination of surfactants OA and dioctylamine (DOA). Further, an Ostwald ripening process was observed in the case of TOPO alone. Complementary electronic structure calculations were used to predict the optimized Co−surfactant complex structures and to quantify the binding energy between the surfactants (ligands) and the Co atoms. These calculations were further applied to predict the Co nanoparticle nucleation and growth processes based on the stability of Co−surfactant complexes.

Introduction

The synthesis of high-quality magnetic nanoparticles has been well-studied over the past decade, owing to their potential applications in various fields, such as high density data storage (e.g., FePt) and biomedicine (e.g., iron oxide).[1,2] Applications of metallic magnetic nanoparticles has been limited by their sensitivity to oxidation. There is a growing interest to explore the potential of metallic magnetic nanoparticles for their high magnetic moments. Synthesis of monodispersed Co nanoparticles in solution has been reported using high-temperature reduction,[3] inverse micelle,[4] and high-temperature injection methods.[5,6] For the high-temperature injection method, the particle size and shape are primarily controlled by the surfactants. It has also been shown that the precursor[7] and reaction temperature[8] can lead to shape control. The crystal structure of spherical Co nanoparticles is mainly epsilon cobalt, a metastable phase with a cubic cell.[9] Extensive studies of nanoparticle formation mechanisms in solution at high temperature have been focused on semiconductors[10,11] and iron oxides.[12,13] Little work has been dedicated to study the formation process of metallic magnetic nanoparticles, primarily due to their propensity for oxidation. Further understanding of metallic nanoparticle synthesis will not only benefit the biological applications that require high magnetic moments[14] but also provide valuable information to other fields, such as catalysis.

It is generally accepted that nucleation and growth are the key steps in the nanoparticle formation process, and the supersaturation level is the driving force to initiate the nucleation events.[15] Simulation performed on semiconductors and iron oxides also suggested that the separation of nucleation and growth is the key to achieve monodispersity.[12] The most acceptable mechanism is the classic LaMer theory, which suggests a burst nucleation followed by a diffusional growth, leading to monodisperse nanoparticles, due to the temporally discrete nucleation.[16] It has also been suggested that nuclei may initially follow diffusional growth to form primary small particles, and then these primary particles aggregate into the final particles; this process is the so-called "aggregation of subunits" mechanism.[17,18] This mechanism can also lead to monodispersity according to this theoretical model, which suggests that the aggregation process is triggered by the elimination of the repulsive barrier and the diffusion rate of the primary particles, leading to size selection. Further, if nucleation is not a one-time event or if nuclei cannot grow at the same time, an Ostwald ripening process will occur.[19] During this process, the smaller particles will dissolve (due to their high surface energy), feeding the growth of larger particles. It remains unclear whether or not a specific particle growth pathway can be selectively achieved.

In this study, we present evidence for different surfactant-mediated growth pathways of Co nanoparticles in a single system. For example, the Co nanoparticles followed a diffusional growth pathway when surfactants oleic acid (OA) and trioctylphosphine

*To whom correspondence should be addressed. E-mail: ybao@eng.ua.edu (Y.B.); kannanmk@u.washington.edu (K.M.K.).

(1) Pankhurst, Q. A.; Connolly, J.; Jones, S. K.; Dobson, J. *J. Phys. D* **2003**, *36*, R167.
(2) Krishnan, K. M.; Pakhomov, A. B.; Bao, Y.; Blomqvist, P.; Chun, Y.; Gonzales, M.; Griffin, K.; Ji, X.; Roberts, B. K. *J. Mater. Sci.* **2006**, *41*, 793.
(3) Murray, C. B.; Sun, S.; Doyle, H.; Betley, T. A. *MRS Bull.* **2001**, 26.
(4) Petit, C.; Taleb, A.; Pileni, M. P. *J. Phys. Chem. B* **1999**, *103*, 1805.
(5) Puntes, V. F.; Krishnan, K. M.; Alivisatos, P. *Appl. Phys. Lett.* **2001**, *78*, 2187.
(6) Puntes, V. F.; Krishnan, K.; Alivisatos, A. P. *Top. Catal* **2002**, *19*, 145.
(7) Dumestre, F.; Chaudret, B.; Amiens, C.; Fromen, M. C.; Casanove, M. J.; Renaud, P.; Zurcher, P. *Angew. Chem., Int. Ed.* **2002**, *41*, 4286.
(8) Cheng, G. J.; Shull, R. D.; Walker, A. R. H. *J. Magn. Magn. Mater.* **2009**, *321*, 1351–1355.
(9) Sun, S. H.; Murray, C. B. *J. Appl. Phys.* **1999**, *85*, 4325.
(10) van Embden, J.; Mulvaney, P. *Langmuir* **2005**, *21*, 10226.
(11) Qu, L. H.; Yu, W. W.; Peng, X. P. *Nano Lett.* **2004**, *4*, 465.
(12) Park, J.; Joo, J.; Kwon, S. G.; Jang, Y.; Hyeon, T. *Angew. Chem., Int. Ed.* **2007**, *46*, 4630.
(13) Kwon, S. G.; Piao, Y.; Park, J.; Angappane, S.; Jo, Y.; Hwang, N. M.; Park, J. G.; Hyeon, T. *J. Am. Chem. Soc.* **2007**, *129*, 12571.
(14) Bao, Y.; Krishnan, K. M. *J. Magn. Magn. Mater.* **2005**, *293*, 15.
(15) Kashchiev, D.; van Rosmalen, G. M. *Cryst. Res. Technol.* **2003**, *38*, 555.
(16) LaMer, V. K.; Dinegar, R. H. *J. Am. Chem. Soc.* **1950**, *72*, 4847.
(17) Park, J.; Privman, V.; Matijevic, E. *J. Phys. Chem. B* **2001**, *105*, 11630.
(18) Privman, V.; Goia, D. V.; Park, J.; Matijevic, E. *J. Colloid Interface Sci.* **1999**, *213*, 36.
(19) Ratke, L.; Voorhees, P. W. *Growth and Coarsening: Ostwald Ripening in Material Processing*; Springer: Berlin, 2002.

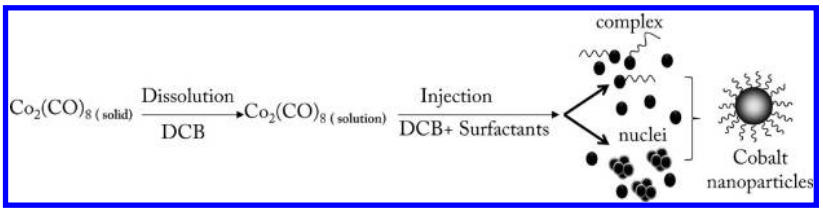

Figure 1. Schematic illustration of the cobalt nanoparticle formation.

oxide (TOPO) were used during the synthesis procedure. Multiple-grained nanoparticles were formed through an aggregation process in the presence of surfactants OA and dioctylamine (DOA). An Ostwald ripening process was observed with surfactant TOPO alone. In conjunction with our electronic structure calculations, these experimental observations can be rationalized by the relative stability of the various Co−surfactant complexes. These results provide an improved understanding of metallic magnetic nanoparticle formation in solution.

Experimental Methods

Chemicals. All chemicals were purchased from Sigma-Aldrich unless otherwise indicated and used without further purification. This includes dioctacarbonyldicobalt containing 1−5% hexane as a stabilizer (Alfa), 1,2-dichlorobenzene (DCB) anhydrous 99%, tri-*n*-octylphosphine oxide (TOPO) 99%, di-*n*-octylamine (DOA) 98%, and oleic acid (OA) 99+%.

Synthesis of Co Nanoparticles. (1) *Single crystalline Co nanoparticles*: 1.58 mmol (0.54 g) of cobalt carbonyl dissolved in 3 mL of DCB was injected into DCB (182 °C) containing a mixture of 0.62 mmol (0.2 mL) of oleic acid and 0.26 mmol (0.1 g) of TOPO, refluxed for 15 min, and then aged for 15 min at a lower temperature (140 °C). (2) *Multiple-grained Co nanoparticles*: 1.58 mmol (0.54 g) of cobalt carbonyl dissolved in 3 mL of DCB was injected into DCB (182 °C) containing a mixture of 0.62 mmol (0.2 mL) of oleic acid and 0.61 mmol (0.34 mL) of DOA, refluxed for 15 min, and then aged for 15 min at a lower temperature (140 °C). (3) *Large* (*20 nm*) *Co nanoparticles*: 1.58 mmol (0.54 g) of cobalt carbonyl dissolved in 3 mL of DCB was injected into DCB (182 °C) containing 0.26 mmol (0.1 g) of TOPO, refluxed for 45 min, and then aged for 15 min at a lower temperature (140 °C).

Characterization. The size and morphology of the Co nanoparticles were characterized with transmission electron microscopy (TEM): a Philips-CM 100 was used for routine bright field imaging, and HRTEM images were obtained with a Philips-CM 200. Samples for TEM analysis were prepared by drying a drop of nanoparticle solution on a carbon-coated copper grid.

Theoretical Methods. All of the electronic structure calculations were performed using Gaussian03.[20] The geometric optimizations of the Co−surfactant complexes were performed using all-electron density-functional theory (DFT), with the popular B3LYP (Becke, three-parameter, Lee−Yang−Parr)[21,22] hybrid exchange-correlation functional. The 6-31+G(d) basis set[23−25] was chosen for Co and the functional groups with lone electron pairs (N, O, and P), while the 3-21G basis set was used for hydrocarbon chains (C and H). The interactions between Co and surfactants (ligand) in which the lone pairs play a key role are well-addressed with the diffuse functions that are included in the 6-31+G(d) basis set. The binding energy (BE) is defined as $BE = [E_{Co-complex} - (E_{Co-atom} + NE_{surfactant})]$, where E is the total energy and N is the ligand coordination number for the Co−complex. Hence, negative (positive) values of BE denote an exothermic (endothermic) binding process.

Results and Discussion

Co nanoparticles were synthesized via thermal decomposition of cobalt carbonyl in a hot solvent containing the surfactant mixture; the details were reported elsewhere.[26,27] In short, the cobalt carbonyl (precursor) dissolved in 1,2-dichlorobenzene (DCB) was injected into hot solvents (DCB, 180 °C) in the presence of various surfactants. Co nanoparticles stabilized by surfactants were then obtained after achieving growth equilibrium. During this process, Co atoms were produced soon after the injection because the reaction temperature (182 °C) was much higher than the decomposition temperature (52 °C) of the cobalt carbonyl precursor.[28] The produced Co atoms were highly reactive, and they either immediately interacted with each other in the locally concentrated environment, forming nuclei containing a number of Co atoms, or they rapidly reacted with surfactants in solution, forming Co−surfactant complexes. The nucleation process stops once the Co monomer concentration drops below the critical supersaturation level. The concentration of the nuclei is determined by the supersaturation level with higher supersaturation level corresponding to higher nucleus concentration.[12] The size of the nuclei is related to the close-shell configuration, the so-called magic sizes.[29] Here, we assume that all of the nuclei are the same size due to the similar experimental conditions. The interactions between the Co atoms and the surfactants can be identified as coordination bonding, in which N and O from the functional groups (e.g., −COOH, $-NH_2$, and −PO) of the surfactants, donated the lone-pair electrons to the partially empty d orbitals of the Co atoms, rendering Co atoms with partial negative charges. The formation process of the Co nanoparticles is illustrated in Figure 1. After nucleation, the reaction solution contains nuclei, free Co atoms, and Co−surfactant complexes.

For a given precursor concentration, the formation of Co−surfactant complexes will directly influence the concentration of Co atoms for nucleation process, the so-called supersaturation level. The nucleation process takes place too rapidly to be experimentally examined or observable on measurement time scale.[12] Therefore, our studies were primarily focused on quantifying the influence of the surfactants on the nanoparticle growth. Three different surfactants of various combinations were studied at fixed precursor (cobalt carbonyl) concentration and fixed reaction temperature. The surfactants used in our study were oleic acid (OA), di-*n*-octylamine (DOA), and tri-*n*-octylphosphine oxide (TOPO), and these surfactants contain an array of different functional groups: carboxylic (−COOH), phosphine

(20) Frisch, M. J. et al. *Gaussian 03, Revision E.01*; Gaussian, Inc.: Wallingford, CT, 2004.
(21) Lee, C. T.; Yang, W. T.; Parr, R. G. *Phys. Rev. B* **1988**, *37*, 785.
(22) Becke, A. D. *J. Chem. Phys.* **1993**, *98*, 5648.
(23) Ditchfield, R.; Hehre, W. J.; Pople, J. A. *J. Chem. Phys.* **1971**, *54*, 724.
(24) Rassolov, V. A.; Ratner, M. A.; Pople, J. A.; Redfern, P. C.; Curtiss, L. A. *J. Comput. Chem.* **2001**, *22*, 976.
(25) Clark, T.; Chandrasekhar, J.; Spitznagel, G. W.; Schleyer, P. V. R. *J. Comput. Chem.* **1983**, *4*, 294.
(26) Bao, Y.; Beerman, M.; Pakhomov, A. B.; Krishnan, K. M. *J. Phys. Chem. B* **2005**, *109*, 7220.
(27) Bao, Y.; Pakhomov, A. B.; Krishnan, K. M. *J. Appl. Phys.* **2005**, *97*, 10J317.
(28) Blums, E.; Cebers, A.; Maiorov, M. M. *Magnetic Fluid*; Walter de Cruyter: Berlin, 1997.
(29) Peng, Z. A.; Peng, X. G. *J. Am. Chem. Soc.* **2002**, *124*, 3343.

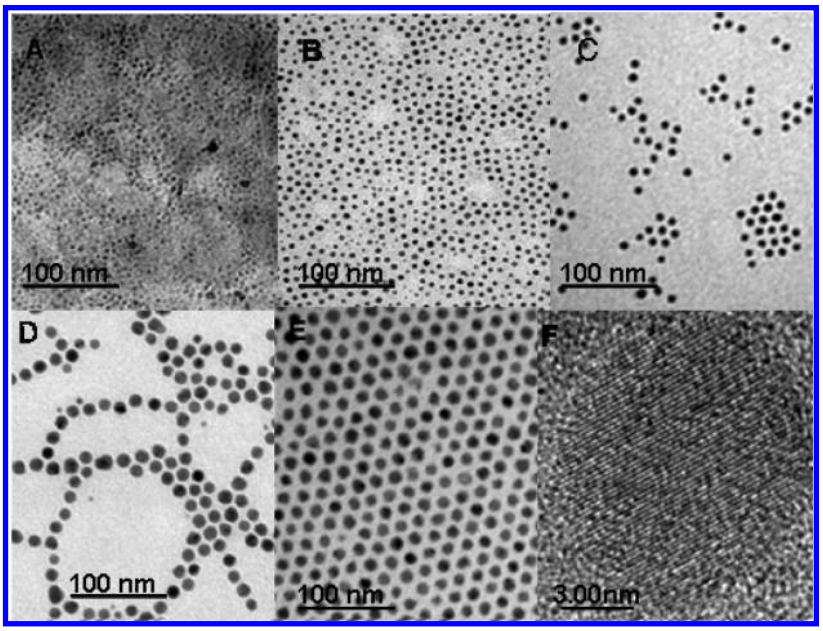

Figure 2. TEM images of the nanoparticles grown in the presence of surfactants OA and TOPO at different stages: (A) 1, (B) 5, (C) 10, (D) 15, and (E) 30 min. (F) High-resolution TEM image showing the highly crystalline particle structures.

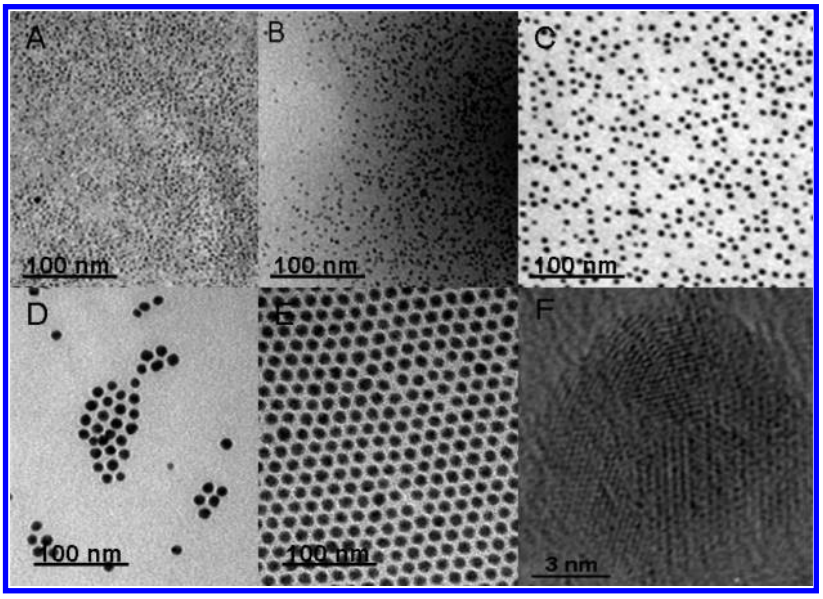

Figure 3. TEM images of nanoparticles grown in the presence of surfactants OA and DOA at different stages: (A) 1, (B) 5, (C) 10, (D) 15, and (E) 30 min. (F) High-resolution TEM image showing the multiple-grained particle structure.

oxide (−PO), and amine ($-NH_2$) groups, respectively. The size and geometrical features of these surfactants are also different. For example, OA has a single $C_{18}H_{33}$ chain with a kink (C═C double bond) at the ninth carbon, TOPO has three C_8H_{17} chains, and DOA has two C_8H_{17} chains. The nanoparticle growth process was studied by extracting fractions of reaction solution at different time intervals and then dropping on grids for TEM observations without any wash or further cleaning. Such TEM samples represent the reaction condition at that particular time.

Figure 2 shows the particle growth process when surfactants OA and TOPO [Co/(OA + TOPO) = 3.5:1; OA/TOPO = 2.3:1] were used. The particle growth process at various reaction stages (1, 5, 10, 15, and 30 min) is depicted in the TEM images of the corresponding samples (Figure 2A−E). At the beginning stage, a dark background with only few particles is observed, likely due to the monomers and the high nuclei concentration. The TEM grid of the sample taken at 1 min was covered with small monodisperse nanoparticles (3−4 nm). The nanoparticle sizes gradually increased with time, but the size distribution was relatively uniform for the duration of the growth; at 15 min, 10 nm Co nanoparticles were formed. Between 15 and 30 min, no significant change in particle size was observed. The crystal structures of the final particles were examined with high-resolution TEM (HRTEM), indicating the formation of single crystalline Co nanoparticles (Figure 2F).

The nanoparticle growth process in the presence of both OA and DOA [Co/(OA + DOA) = 2.5:1; OA/DOA = 1:1] is illustrated in Figure 3. The TEM images of the nanoparticles at different reaction stages (1, 5, 10, 15, and 30 min) are presented in Figure 3A−E. A uniform size distribution of the nanoparticles was observed throughout all the stages, but with an increase in particle size. However, the final 10 nm nanoparticles exhibited

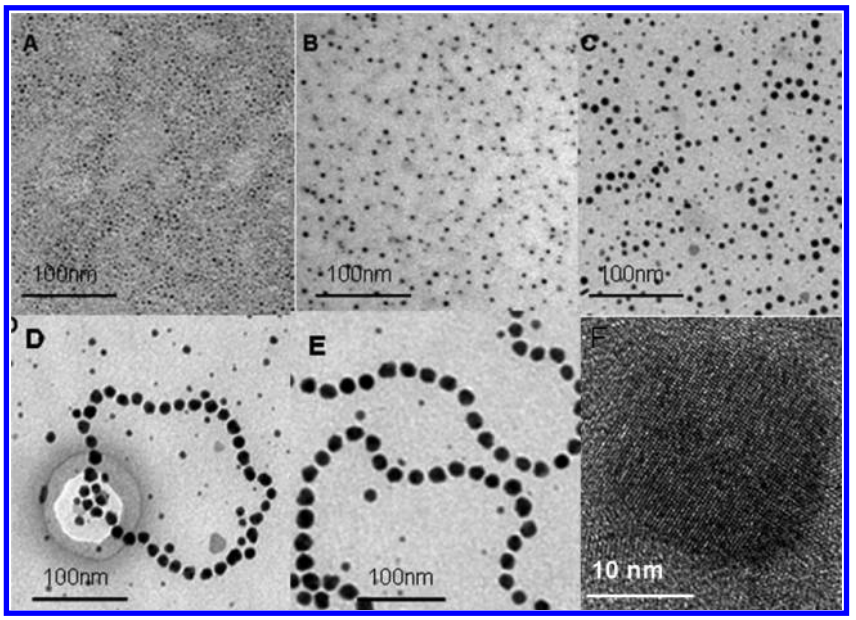

Figure 4. TEM images of nanoparticles grown in the presence of surfactant TOPO alone at different stages: (A) 1 min, (B) 5 min, (C) 15 min, (D) 30 min, and (E) 1 h. (F) HRTEM image showing the single crystalline structure.

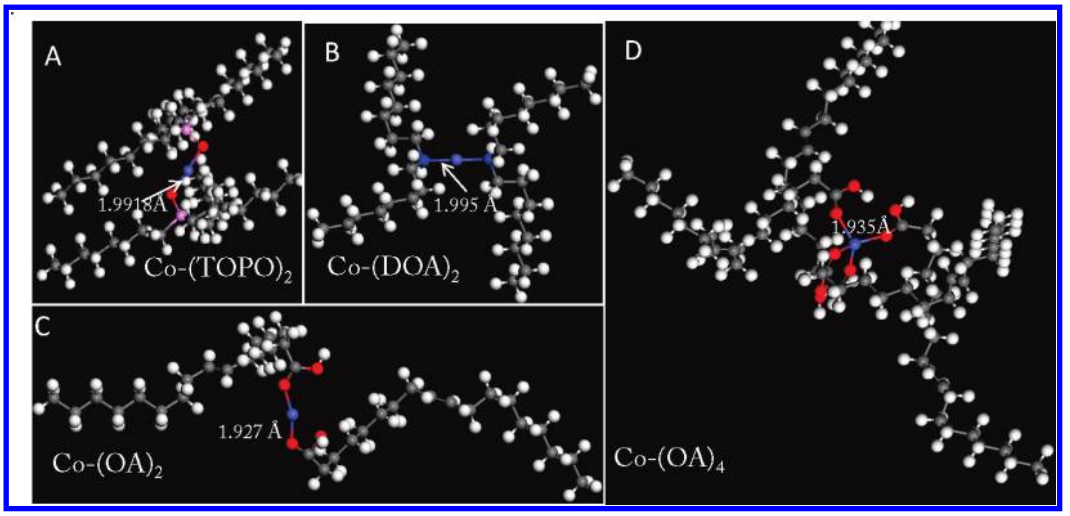

Figure 5. Optimized structures of Co−surfactant complex: (A) Co−$(TOPO)_2$, (B) Co−$(DOA)_2$, (C) Co−$(OA)_2$, and (D) Co−$(OA)_4$.

multiple-grained crystal structures, evidenced by the HRTEM image, where the grain boundaries inside the particle can be clearly seen (Figure 3F). As shown in Figure 4, the particle evolution process with TOPO (Co/TOPO = 12:1) alone exhibits a wide particle size distribution during the early stages of the reaction, but the growth evolved toward the final particles with an increase in size. Figure 4A−D shows the nanoparticle morphologies at reaction times of 1, 5, 15, and 30 min. With increased reaction time, nanoparticles with a reasonably narrow size distribution were observed (Figure 4E). Compared to the other two systems, larger 20 nm Co nanoparticles with single crystalline structures were synthesized (Figure 4F). The Co nanoparticles synthesized using the single TOPO surfactant were not stable at room temperature in air. This is most likely due to the presence of the bulky chains of the TOPO surfactants, which prevents them from packing tightly on the surface.[26] This was corroborated with an HRTEM image, which showed a surface oxidation layer of 1−2 nm. A rough calculation of the lattice spacing from the HRTEM image gave a value of 0.215 nm, which corresponds to the (200) planes of the CoO lattice. The oxidation was also confirmed with XRD scans (Supporting Information, Figure S1).

Table 1. Calculated Binding Energy of the Co−Surfactant Complexes

Co complex	binding energy, BE (eV)
$Co(TOPO)_2/Co\{[CH_3(CH_2)_7]_3PO\}_2$	−0.92
$Co(DOA)_2/Co\{[CH_3(CH_2)_7]_2NH\}_2$	−1.51
$Co(OA)_2/Co[CH_3(CH_2)_7CH{=}CH(CH_2)_7COOH)]_2$	+0.73
$Co(OA)_4/Co[CH_3(CH_2)_7CH{=}CH(CH_2)_7COOH)]_4$	−0.61

Co nanoparticles with epsilon crystal structures were produced from all three processes regardless of the nanoparticle sizes and crystallinity based on XRD scans (Supporting Information, Figure S1). The formation of Co nanoparticles with different crystallinity suggested different growth pathways, which is influenced by the surfactant species. After the Co atoms were produced in the reaction, the nucleation and the Co−surfactant complex formation were the two competing processes present in the mixture. The nucleation event was mainly driven by the

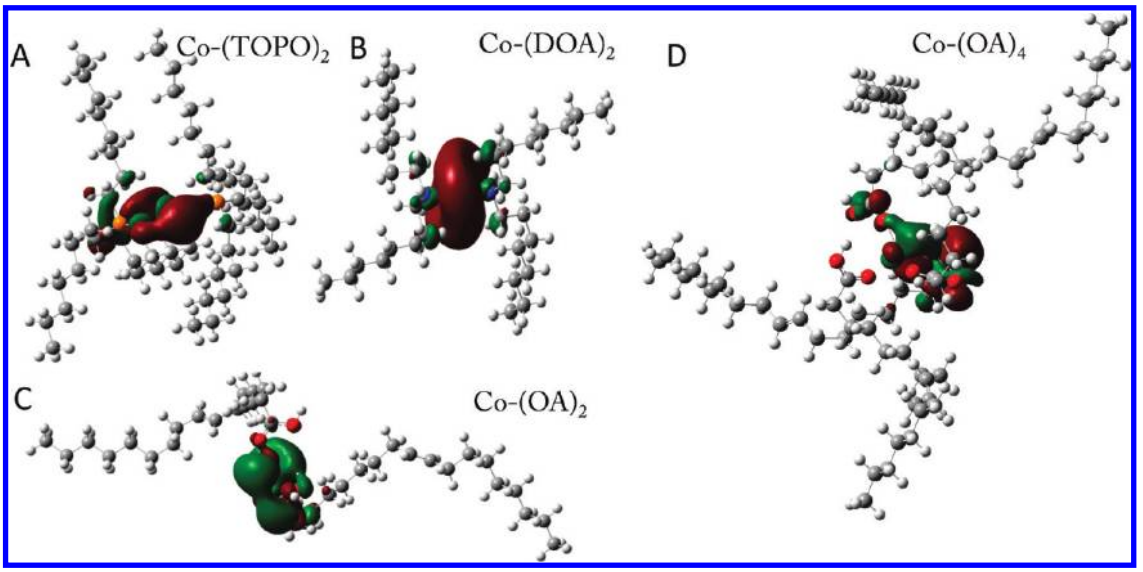

Figure 6. Calculated isosurfaces (isovalue = 0.02 e/Å^3) of the HOMO for Co−surfactant complexes: (A) Co−$(TOPO)_2$, (B) Co−$(DOA)_2$, (C) Co−$(OA)_2$, and (D) Co−$(OA)_4$.

supersaturation level of the Co atoms, which was influenced by the formation of the Co−surfactant complexes. Further nanoparticle growth was determined by the relative populations of nuclei, free Co atoms, and Co−surfactant complexes as well as the stability of the Co−surfactant complexes. The growth of nanoparticle stops when the monomers are depleted or the nanoparticle surfaces are well stabilized by surfactants.

In order to gain more insight into the effects of surfactants on the growth of the Co nanoparticles, we calculated the binding energy (BE) at 0 K for the Co−surfactant complexes using all-electron DFT method. The optimized structures of the Co complexes with OA, TOPO, and DOA as ligands are shown in Figure 5. It can be seen that 13-electron Co−surfactant complexes were formed via the coordination of two surfactant molecules and a Co atom, which are both neutral. It has been reported that electronically unsaturated Co(II) complexes are thermally stable in solution.[30] Considering their same coordinate bonding nature, such two-coordinated Co−surfactant complexes with sizable binding strength are expected to be produced during the synthesis process. The single surfactant coordination was not favored due to the higher system energy, compared to the two coordination configuration. A higher ligand coordination number was excluded for TOPO and DOA due to their bulky size and position of functional group, which led to an unstable configuration during the optimization; thus, the calculation could not be completed. Interestingly, a 17-electron stable $Co(OA)_4$ complex is formed during our simulation, which is much more stable than two- and three-coordination complexes because of the formation of a tetrahedral geometry CoO_4 core and hydrogen bonding among −OH groups, which is not sustainable at high temperature. The calculated BEs are listed in Table 1. It can be seen that the BEs for $Co(DOA)_2$, $Co(TOPO)_2$, $Co(OA)_2$, and $Co(OA)_4$ are −1.51, −0.92, 0.73, and −1.21 eV, respectively. Note that negative (positive) values of BE correspond to an exothermic (endothermic) binding process. The negative value of $Co(OA)_4$ and the positive value of $Co(OA)_2$ suggest that $Co(OA)_4$ is more stable than $Co(OA)_2$ (Table 1). In addition, once two ligands leave the complex, the detachment of the other two from Co atoms will become a favorable and spontaneous process. The isosurface of the HOMO for each Co−surfactant complexes is shown in Figure 6. It is apparent that the HOMO is mainly localized around the Co atoms, which were subject to further reaction with Co nuclei during the association process.

In the cases of OA/TOPO, ∼15% (estimated from the relative concentration of cobalt carbonyl and surfactants; see Supporting Information for detailed calculation) of the Co atoms could form complexes, and the remaining 85% of the Co atoms were available for the nucleation process. The supersaturation level is related to the free atoms in the reaction, which will then directly influence the nucleus concentration. The Co atoms experienced three dominant processes during reaction: rigorous nucleation, formation of $Co(TOPO)_2$ complexes, and formation of $Co(OA)_4$ complexes. Our calculation showed that the formation of $Co(OA)_2$ is an endothermic process, but the formation of $Co(OA)_4$ is exothermic, which suggests that once two ligands leave the Co atoms, the other two will detach spontaneously. Therefore, the BE is compared using two ligand binding numbers, and so does the percentage calculation. The nucleation events stopped when the Co concentration dropped below the critical concentration. The formation of 10 nm single crystalline nanoparticles could be explained by the diffusional growth until depletion of free cobalt atoms, followed by continuous growth via the dissociation of Co−surfactant complexes. The similar binding energies of $Co(OA)_4$ and $Co(TOPO)_2$ complexes allow simultaneous growth of the Co nanoparticles until all the Co atom sources are depleted. The rapid nucleation and diffusional growth process were similar to the classic LaMer theory.[16]

Similarly, in the case of OA and DOA, the Co nuclei, free Co atoms, and Co−$(OA)_4$, and Co−$(DOA)_2$ complexes were formed with ∼19% Co−surfactant complexes. Initially, all of the nuclei could grow to a certain size via quick depletion of free Co atoms. Further continuous diffusional growth cannot simultaneously proceed because of the slow release of the Co atoms from the relatively stable $Co(DOA)_2$ complexes. To minimize the surface energy of the small nanoparticles, a simultaneous process of aggregation of small particles and continuous growth took place, a process similar to the mechanism of the so-called "aggregation of subunits".[17,18] Because of the aggregation, multiple-grained nanoparticles were formed (Figure 4F). This multigrained struc-

(30) Holland, P. L.; Cundari, T. R.; Perez, L. L.; Eckert, N. A.; Lachicotte, R. J. *J. Am. Chem. Soc.* **2002**, *124*, 14416.

ture was also confirmed with XRD scan, indicated by the peak broadening (Supporting Information, Figure S1).

For the TOPO only system, a high concentration of nuclei are spontaneously formed due to the high level of the supersaturation (96% atoms), which did not allow for all of the nuclei to continuously grow at the same time, resulting in a wide particle size distribution. From the thermodynamic point of view, the smaller particles will have a greater tendency to dissolve due to their high surface energy, feeding the growth of larger particles; this is the so-called Ostwald ripening process.[19] During the dissolution of the smaller particles and the growth of larger particles, larger nanoparticles were obtained with increasing reaction time. For the same amount of precursor, 20 nm Co nanoparticles were obtained after 1 h, but the size distribution is not as narrow as the two surfactant systems. In addition, the diffusional growth leads to single crystalline nanoparticles. Experiments using only OA and DOA were also conducted, but not included in this work, because the synthesis was not able to produce controllable nanoparticles, such as wide size distribution. In brief, the relative stability and concentration of the Co−surfactant complexes play a critical role in the mechanistic growth of cobalt nanoparticles.

Conclusion

Using the synthesis of Co nanoparticles as a model system, we have demonstrated the important roles of surfactants in nanoparticle nucleation and growth, by affecting the concentrations of the nuclei and surfactant complexes. The variation in the concentration of nuclei and complexes resulted in different nanoparticle growth pathways, leading to various morphologies. In a single system, three different growth pathways of Co nanoparticles were observed (by varying the surfactants): diffusional growth, aggregation, and Ostwald ripening. In conjunction with our electronic structure calculations, we suggest that the concentration of the surfactants and their relative bond strength with Co atoms are the variables responsible for altering the nanoparticle growth processes. This study provides valuable information for controlling nanoparticle morphologies, which may possibly be generalized to other nanoparticle systems.

Acknowledgment. This work was supported by NSF grants DMR-0501421 and DMR-0203069 at UW. We thank Pacific Northwest National Laboratory and Lawrence Berkeley National Laboratory for use of the TEM facilities. C.H.T. and W.A. acknowledge supercomputer resources provided by the Alabama Supercomputer Center, NCSA TeraGrid, and the Pacific Northwest National Lab EMSL facility; Y.B. acknowledges the UA-COE start-up funds.

Supporting Information Available: Calculations of Co−surfactant complex concentrations and XRD scans of Co nanoparticles. This material is available free of charge via the Internet at http://pubs.acs.org.